KSCE Journal of Civil Engineering (0000) 00(0):1-8
DOI 10.1007/s12205-015-0363-7

Geotechnical Engineering
pISSN 1226-7988, eISSN 1976-3808
www.springer.com/12205

Numerical Simulation of Centrifuge Experiments on Liquefaction Mitigation of Silty Soils using Stone Columns

Liang Tang*, Xiaoyu Zhang, and Xianzhang Ling*****

Received July 4, 2014/Revised September 1, 2014/Accepted April 30, 2015/Published Online July 7, 2015

Abstract

Installation oF Stone Column (SC) is a promising ground improvement technique to mitigate liquefaction hazards in sand stratum. In this study, a three-dimensional (3D) Finite Element (FE) analysis was used to simulate a centrifuge experiment on the mitigation of silty sand strata liquefaction using SC approach. The predicted response of the silty sand and SC matched the experimental data well. The overall site-stiffening effects due to the installed SCs as well as the distributions of the shear stress and shear stress reductions were evaluated. A parametric study was conducted to investigate the effect of the SC permeability and the surface load at the SC zone on the effectiveness of liquefaction mitigation. The results showed that the SCs behaved in a combined shear and flexure mode. Furthermore, the SCs with permeability exceeding a threshold value can dramatically decrease the liquefaction hazard. On the other hand, larger surface load did not prevent soil liquefaction and produced negligible benefits in stiffening. The present study further enhances the current understanding of the effectiveness of SC remediation approaches in the silty sand.

Keywords: *earthquake, ground improvement, liquefaction, stone column, finite element, centrifuge modeling*

1. Introduction

Liquefaction can cause major damages and destruction to foundations and associated building, bridge, and embankment as reported in past earthquake events around the world (Adalier *et al.*, 2003; Baez and Martin, 1995; Mitchell, 2008). Several methods, such as gravel drains/Stone Columns (SCs), densification, and solidification, are commonly used to reduce the risk of liquefaction and the associated ground deformation (Baez, 1995; Adalier *et al*., 2003; Mitchell, 2008). Among these methods, the SC technique is preferred for the mitigation of liquefaction hazards because of its effectiveness and the simple construction involved (Adalier *et al*., 2003).

Seed and Booker (1977) initially evaluated the use of SCs for improving the liquefaction resistance of liquefiable sand. Recently, extensive research efforts have to assess the effectiveness of SCs for liquefaction mitigation of the sand using field case histories (Mitchell and Wentz, 1991), limited centrifuge and shake-table experiments (Adalier *et al.*, 2003; Martin *et al*., 2003), and numerical simulation (Elgamal *et al*., 2009; Lu *et al*., 2011).

Generally, improvement of the liquefaction triggering resistance of soil using SCs can be considered through three mechanisms: densification, drainage, and reinforcement (Shenthan *et al*., 2004). The reinforcement mechanism due to the introduction of the stiffer SCs is considered to be more effective for silty sand and non-plastic silty soil, where the combined use of densification and drainage are difficult to achieve to counteract seismic-induced liquefaction (Baez, 1995). However, the beneficial effects due to the installed SCs for the liquefaction mitigation of silty soils have not been fully addressed yet (Olgun and Martin, 2008; Rayamajhi *et al*., 2014).

Moreover, current design practice for the SCs assumes that stiff columns deform compatibly in shear with the surrounding soil (Baez, 1995). The implication of this assumption is that the SCs, being stiffer than the existing soil, would attract higher seismic shear stresses than the existing soil, thus expected to improve the liquefaction triggering resistance.

Nevertheless, other studies have concluded that discrete columns may undergo flexure and shear deformation thus becoming less effective in the reduction of shear stresses than the shear strain compatibility assumption implies (Goughnour and Pestana, 1998). Published researches (Green *et al.*, 2008; Olgun and Martin, 2008; Rayamajhi *et al.*, 2014) also suggest that flexure response may dominate near the ground surface while shear response may dominate at deeper depths. However, the levels of shear stress and the strain distributions in the surrounding silty soil have not been fully understood.

A series of dynamic centrifuge experiments were performed to further investigate the dynamic characteristics of silty soils with and without a surface foundation surcharge (Adalier *et al*., 2003).

*Aassociate Professor, School of Civil Engineering, Harbin Institute of Technology, Harbin, China (Corresponding Author, E-mail: hit_tl@163.com)
**Ph.D. Student, School of Civil Engineering, Harbin Institute of Technology, Harbin, China (E-mail: zxy_hit@163.com)
***Professor, School of Civil Engineering, Harbin Institute of Technology, Harbin, China (E-mail: xianzhang_ling@263.net)

Recently, 3D FE simulations have increasingly emerged as a versatile tool to study this issue. In the following sections, an experiment to be simulated is briefly described. Next, the numerical modeling procedure used to simulate the experiment was explained, and the reinforcement effect, shear stress and strain distributions obtained from the FE results were discussed. Subsequently, a parametric study was conducted to highlight the effect of the SC permeability and surface load at the SC zone on the mitigation of liquefaction. Finally, some insights and conclusions are drawn.

2. Description of the Experiment

The main principle in centrifuge physical modeling is that a 1/N (N is level of gravitational acceleration) scale model subjected to a gravitational acceleration of Ng (g is acceleration of gravity) experiences the same stress level and stress distribution as the prototype. Unless otherwise indicated, all dimensions reported in this paper are given in prototype scale, obtained from the actual model units following basic scaling relations (Tan and Scott, 1985).

Figure 1 shows a benchmark centrifuge experiment on the potential mitigation of liquefaction of silt strata by the SCs to be simulated in this study (Adalier *et al*., 2003). The model was tested at a 50 g gravitational acceleration field. A rectangular laminar box with flexible walls was used. Ground water table was at the soil surface initially.

The experimental model consisted of a single 7.8-m thick layer of saturated silty sand. 100% silt size particulate material (Sil-Co-Sil 120, Walker and Stewart, 1989) was employed to construct the ground layer. At a relative density (D_r) of 60%, the internal friction angle of this silty sand is estimated to be 25 degree. Water permeability of the Sil-Co-Sil 120 Silt tested conventionally in the 1 g laboratory (at D_r of around 60%) is roughly 8.67×10^{-8} m/s. In view of the scaling laws applicable to the centrifuge experiment, the prototype permeability of the salty sand at 50 g is 4.3×10^{-6} m/s.

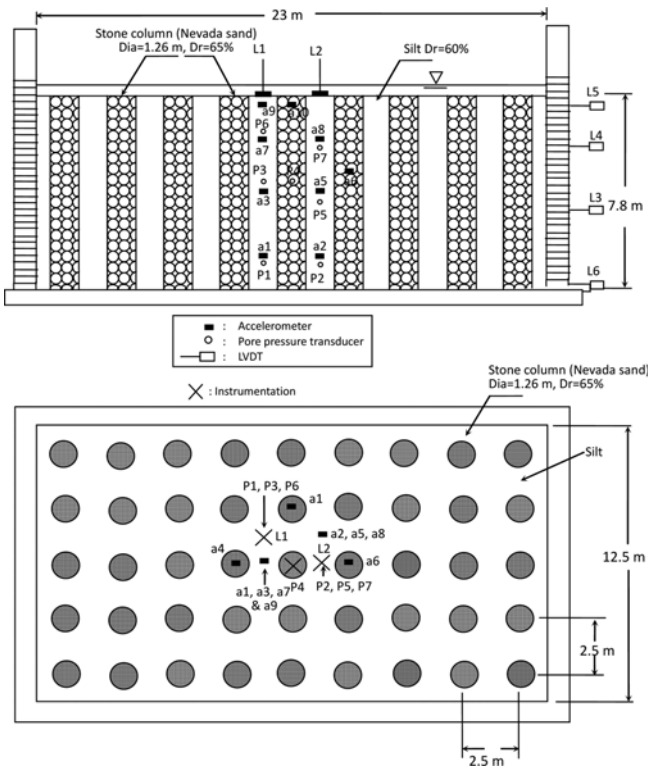

Fig. 1. View of the Centrifuge Experiment (after Adalier *et al.*, 2003)

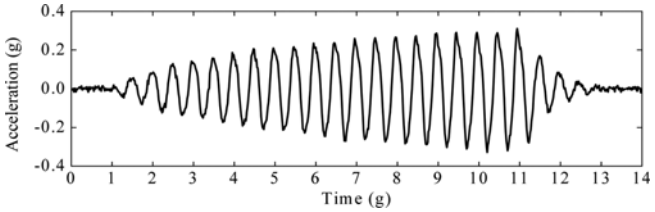

Fig. 2. Base Input Motion

The material representing the SCs was Nevada No. 120 sand (Arulmoli *et al*., 1992). The SCs with a void ratio of about 0.62 (about D_r of 65%) were prepared for the experiment. Water permeability of the sand tested conventionally in the 1 g laboratory (at D_r of about 65%) is 5.2×10^{-5} m/s (roughly 600 times more permeable than Sil-Co-Sil 120 Silt) therefore the prototype permeability of the sand at 50 g should be 2.6×10^{-3} m/s. Internal friction angle of this sand is estimated to be 37 degree.

Overall, 45 SCs that were 1.27 m in diameter were placed vertically with 2.5 m between their centers at the specified positions, giving an area replacement ratio (A_r) of 20% where the area replacement ratio is defined as the area of the SC to the tributary area per SC (Elgamal *et al*., 2009).

During the testing phase, each SC was encased in a 0.015-m thick latex membrane. At the SC base, the membrane was sealed with silicon glue and end-cap circular plastic plates of 0.25-m thickness and 1.27-m diameter. For detailed descriptions of typical model preparation techniques, instrumentation, and testing procedures, the reader is referred to Adalier *et al*. (2003).

The model was excited using a sinusoidal base acceleration with increasing amplitude for 20-cycles and at a dominant frequency of approximately 1.8 Hz (see Fig. 2). Model response was measured by miniature transducers, including accelerometers and pore pressure transducers.

3. Numerical Modeling

All FE simulations were performed using the open-source computational platform OpenSees (http://opensees.berkeley.edu, Mazzoni *et al.*, 2009) with the aid of OpenSeesPL as a pre- and post-processing tool (Lu *et al*., 2011) to efficiently perform the simulation using OpenSees.

3.1 Finite Element Model

Typical SCs see Fig. 3 were constructed in a grid pattern to improve the silt stratum covering the entire building footprint. A "unit cell" (i.e., a representative area of improved soil) with a periodic boundary (Law and Lam, 2001) is used to model the

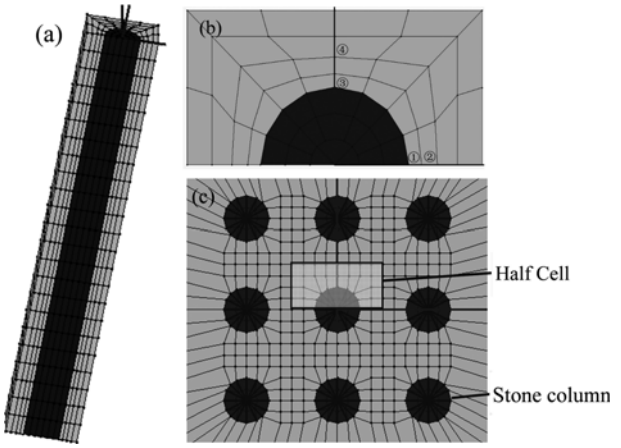

Fig. 3. Improved FE Element Model with Stone Columns: (a) 3D Isometric View with 1/2 Mesh, (b) Plan View, (c) Stone Column Layout

remediated area with a large spatial extent.

Considering symmetry considerations, a half-mesh configuration as shown in Fig. 3 was used to simulate the experiment. The boundary conditions imposed on the FE model are given below: (1) the penalty method was used to set equal displacement degrees of freedom for the corresponding left and right boundary nodes at any spatial location in the horizontal and vertical directions (i.e., periodic boundary as imposed by the laminar box); (2) the inner (symmetric) and outer boundaries were fixed against out-of-plane displacement but are free to move longitudinally and vertically; (3) the soil surface was stress-free; (4) the recorded sinusoidal base acceleration from the experiment (see Fig. 2) was applied to the base of the FE model along the shaking direction.

The FE modeling of the soil and the SC was conducted using a 20-8 noded, effective-stress solid-fluid fully coupled brick element (Biot, 1955; Zienkiewicz *et al.,* 1990; Lu *et al*., 2011). This element is based on the solid-fluid formulation for saturated soil (Biot, 1955; Zienkiewicz *et al.*, 1990). A total of 20 nodes were used to describe the solid translational degrees of freedom, and 8-corner nodes are used to represent the fluid pressure. To model the experiment satisfactorily, a multi-yield-surface plasticity constitutive relationship were selected to model the SC and soil (Elgamal *et al.*, 2003; Parra, 1996; Yang, 2000). In the numerical analyses, 3% Rayleigh damping was employed for both the improved and unimproved cases (Rayamajhi *et al*., 2014).

3.2 Benchmark Cases SC and SS

A parametric study on the material parameters was performed, and Table 1 shows the parameters for the silty sand and the SC used in the FE model which produced reasonable agreement with the experimental data. Based on these parameters, the SCs were employed to improve the performance of the silt stratum using the benchmark models as Case SC. Meanwhile, the silty sand case (Case SS) represents the benchmark of the original unremediated situation. The results of Case SS serve as a reference for the free-field response.

Table 1. Soil Model Parameters

Parameters	Silty soil	Gravel sand (used for stone columns)
Mass density (kg/m^3)	1700	2000
Low-strain shear modulus G_r (at 80 kPa mean effective confinement, MPa)	15.7	78.5
Friction angle ϕ	25°	37°
Liquefaction yield strain γ_y	0.005	0
Contraction parameter c_1	0.15	0.05
PT angle γ_{PT}	23°	30°
Dilation parameter d_1	0.2	0.4
Dilation parameter d_2	10	10
Permeability (m/s)	4.3×10^{-6}	2.6×10^{-5}

4. Results of Benchmark Case SC

Figures 4 and 5 illustrate the computed and experimental excess pore pressure (u_e) and acceleration time histories of the silty soil, respectively. The computed and experimental acceleration and u_e within the SC are shown in Fig. 6.

The numerical and experimental excess pore pressures at two depths were in close agreement with each other. The u_e accumulation initially was rapid and reached a peak, and subsequently attained a nearly constant high level up to the end of shaking (Fig. 4). It implies that full liquefaction at these depths was reached after about 12-16 cycles of shaking. However, the maximum excess pore pressure ratio, r_u, which is the ratio of the u_e to the initial overburden vertical effective stresses attained inside the SC (Fig. 6) at a depth of 4.0 m was less than 0.5, followed by a relatively quick reduction of the u_e after around 9.5 s.

As seen from Fig. 5, the benchmark model simulated the experimental acceleration at the depths of 4.3 m and 6.7 m well. The accelerations of the silty sand at a depth of 4.3 m began to significantly decrease upon the onset liquefaction. Similarly, the acceleration of the SC appeared to increase and then vanish until the shaking ended. However, the amplitude of the soil accelerations

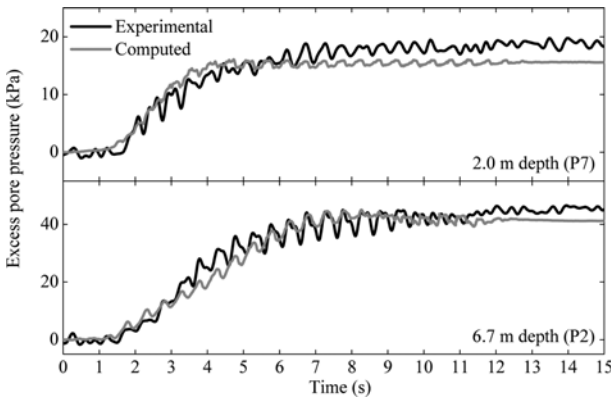

Fig. 4. Experimental and Computed Excess Pore Pressures of the Silty Sand for Case SC (the initial effective vertical stresses for depths of 2.0 and 6.7 m are 14 and 46.9 kPa, respectively)

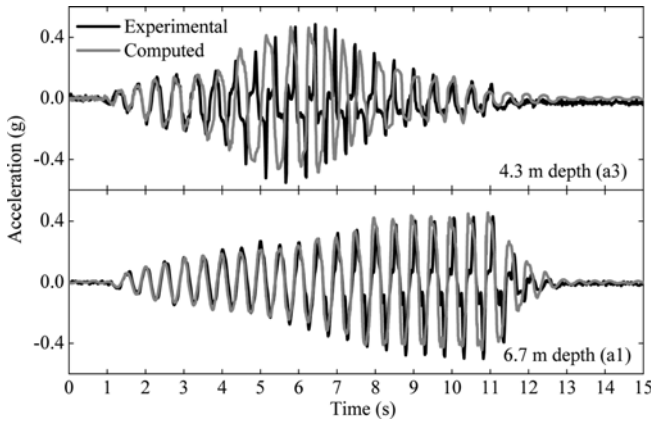

Fig. 5. Experimental and Computed Accelerations of the Silty Sand for Case SC

at 6.7-m depth near the bottom of the soil was gradually increased until the end of shaking. The magnitude and shape of the computed and recorded accelerations were similar to those of the base motion.

5. Parametric Study

5.1 Reinforcement Effects of the SCs

The results of Cases SS and SC are compared to investigate the reinforcement effects due to the SCs. Fig. 7 shows the acceleration time histories of the silty sand for Cases SC and SS. The u_e time histories of the silty sand are presented in Fig. 8 for Cases SC and SS. Some noticeably different behaviors were identified in Cases SS and SC. In Cases SC and SS, soil softening due to the u_e initially accelerated the amplification of acceleration in the silty soil prior to liquefaction. However, the soil accelerations appeared to decrease upon liquefaction because of the reduction of soil stiffness. In addition, subsequent acceleration attenuations were observed earlier in Case SS relative to Case SC. At a depth of 6.7 m, no attenuation can be observed in the silty soil for Case SC.

The time histories of excess pore pressure in the upper half of

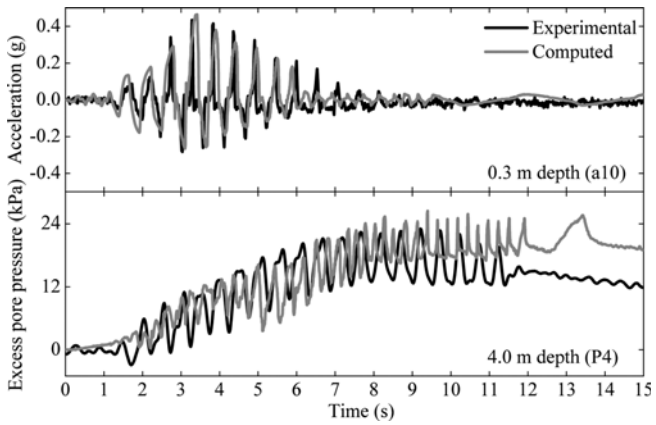

Fig. 6. Experimental and Computed Acceleration and the Excess Pore Pressure in SC for Case SC (the initial effective vertical stress at a depth of 4 m is 40 kPa)

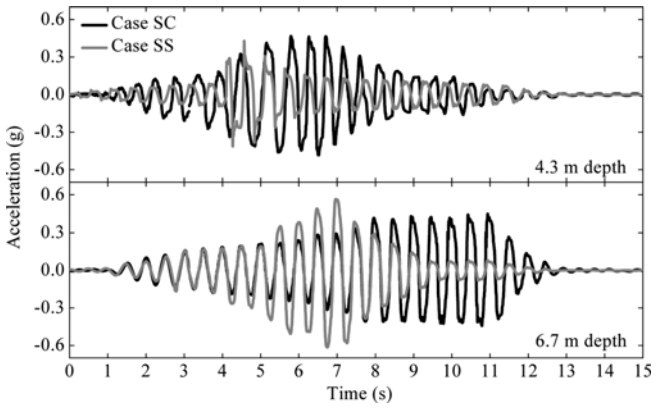

Fig. 7. Acceleration Time Histories of the Silty Sand for Cases SC and SS

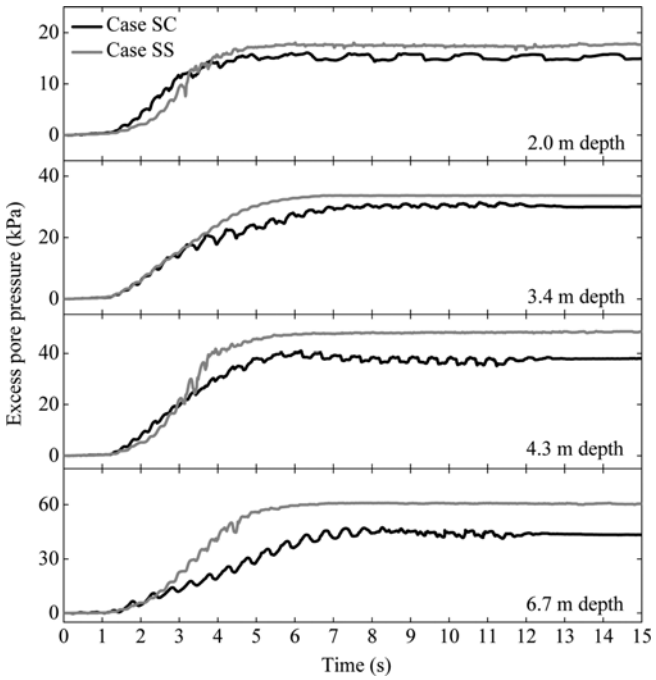

Fig. 8. Excess Pore Pressure Time Histories of the Silty Sand for Cases SC and SS (the initial effective vertical stresses at depths of 2.0, 3.4, 4.3, and 6.7 m are 14.0, 23.8, 30.1 and 46.9 kPa, respectively)

the silty sand in Cases SS and SC were similar (Fig. 8). However, the u_e generation rates in the bottom-half of the silty sand were different between Cases SS and SC. Apparently, the SCs induced a marginal effect in retarding the rise in u_e in the silty sand below approximately 4.3 m.

The entire silty stratum was completely liquefied in Case SS, whereas, only the upper half of the stratum was liquefied in Case SC. Furthermore, as compared to Case SS, an additional two or three shaking cycles at the top half of the silt stratum were required for liquefaction and significant strength degradation to occur in Case SC.

Consequently, although liquefaction in the upper half of the silt stratum could not be prevented by the installation of SCs under the strong input motion, the mitigated ground was considerably

more resistant to liquefaction than the unimproved uniform silty sand because more shaking cycles were required to attain soil liquefaction. This resistance contributed to the increased overall stiffness of the improved ground.

5.2 Shear Stress and Strain Distributions

5.2.1 Deformation Behavior

Figure 9 shows the shear strain (γ) and flexure (θ) deformation of the SC for Case SC. As previously observed, the SC behaved in both shear and flexural modes, which differed from the current design consideration, which assumes that the SCs and the surrounding soil only undergo shear deformation during earthquakes. The shear and flexural deformations initially increased with depth before decreasing at greater depth. The maximum flexural and shear deformations appeared at depths of 6.3 and 5.2 m, respectively. The contributions of the shear deformation were dominant relative to flexural deformation due to the presence of the driving shear stress component. A combined shear and flexure deformation mechanism decreased the shear stress in the surrounding soil due to shear reinforcement, which should produce a greater liquefaction resistance in comparison to the current design consideration.

5.2.2 Shear Stress Distributions

Seed and Idriss (1971) proposed a simplified procedure for calculating the cyclic shear stress ratio (CSR_U) for liquefaction triggering evaluations of unimproved soils (Rayamajhi *et al.*, 2014). This procedure is expressed in the following equation:

$$CSR_U = \frac{\tau_{S,U}}{\sigma_v'} = 0.65\left(\frac{a_{\max,U}}{g}\right)\left(\frac{\sigma_v}{\sigma_v'}\right)r_{d,U} \quad (1)$$

where $\tau_{S,U}$ is the average cyclic shear stress of the soil, σ_v' is the effective vertical stress of the soil, σ_v is the total vertical stress of the soil, $a_{\max,U}$ is the maximum ground surface acceleration, $r_{d,U}$ is the shear stress reduction coefficient ($r_{d,U} = (\tau_{\max})_{d,U}/(\tau_{\max})_{r,U}$, $(\tau_{\max})_{r,U} = \gamma' z a_{\max,U}$), $(\tau_{\max})_{d,U}$ is the maximum shear stress, and γ' is the effective unit weight of the soil.

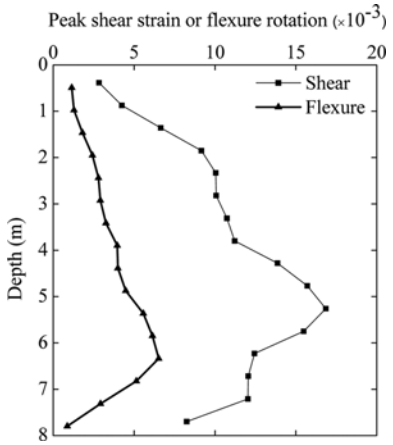

Fig. 9. Shear and Flexure Deformation Patterns of the SC for Case SC

Similarly, the *CSR* for the improved ground (CSR_I) was obtained using Eq. (2),

$$CSR_I = \frac{\tau_{S,I}}{\sigma_v'} = 0.65\left(\frac{a_{\max,I}}{g}\right)\left(\frac{\sigma_v}{\sigma_v'}\right)r_{d,I} \quad (2)$$

where $a_{\max,I}$ could be evaluated by using the average area-weighted ground surface acceleration. The $r_{d,I}$ parameter is a stress reduction coefficient that considers the flexibility of the SC. $r_d = 1$ indicates rigid body behavior.

The ratio of CSR_I to CSR_U is called as the "CSR Reduction Factor" and is related to the dependent-depth and the ratio of the maximum ground surface accelerations as follows:

$$R_{CSR} = \frac{CSR_I}{CSR_U} = \left(\frac{a_{\max,I}}{a_{\max,U}}\right)\left(\frac{r_{d,I}}{r_{d,U}}\right) = R_{a,\max}R_{rd} \quad (3)$$

where R_{rd} is the ratio of the shear stress reduction coefficient for the improved and unimproved soils, and $R_{a,\max}$ is the ratio of the maximum ground surface acceleration. The two main effects of the SCs that result from shear and flexible deformations can be distinguished using Eq. (3).

The ratio of the shear strains between the SC and the surrounding soil is expressed as the shear strain ratio (γ_r). Fig. 10 presents the profiles of R_{rd} and γ_r for Case SC. A lower R_{rd} indicates a lower ground liquefaction potential. The R_{rd} and γ_r vary spatially with vertical and horizontal location. The average R_{rd} decreases linearly with depth. The shear stresses of the silty sand near the SC perimeter are slightly different from those that are not neighboring the SC on the x-axis. Nevertheless, the soil near the SCs sustains lower shear stress than the soil that is not close to the SC and is perpendicular to the shaking direction. The shear stresses of the surrounding soils parallel to the shaking direction are greater than those perpendicular to the shaking direction. Overall, the shear stress level of the surrounding soil is reduced by the installed SCs.

Similarly, the γ_r of the surrounding soil region near the SC parallel and perpendicular to the shaking direction [Fig. 10(b)] tends to increase linearly with depth from the ground surface. In addition, γ_r increases from approximately 0.05 at the ground surface to approximately 0.8 at a depth of 7.8 m. The soil experiences greater shear strain near the SCs than away from the SCs along the y-axis. In contrast, the shear strains of the soils are lower near the SCs than the shear strains of the soils that are further away from the SC on the x-axis. Generally, the SCs decrease the shear strain of the soil and restrict lateral ground deformation.

5.3 Influence of the SC Permeability

Additional numerical analyses were conducted to consider the variation of the SC permeability using the parameters given in Table 1. Apart from the benchmark case with a permeability of 2.6×10^{-5} m/s, cases with permeability of 2.6×10^{-4}, 2.6×10^{-3}, 2.6×10^{-2} and 2.6×10^{-1} m/s were also considered.

Figures 11 and 12 respectively compare the u_e and the ground

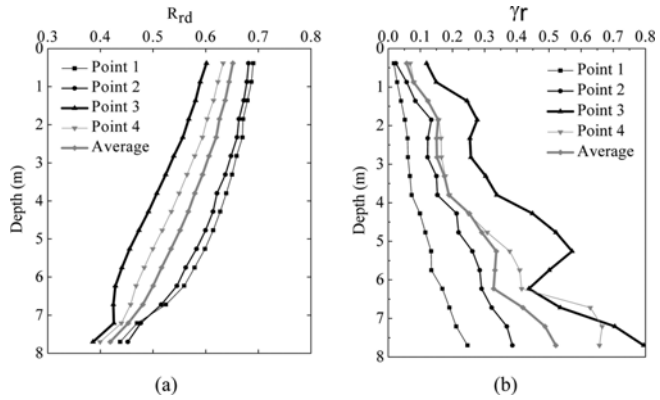

Fig. 10. Computed R_{rd} and γ_r Profiles for the Improved Soil: (a) R_{rd}, (b) γ_r

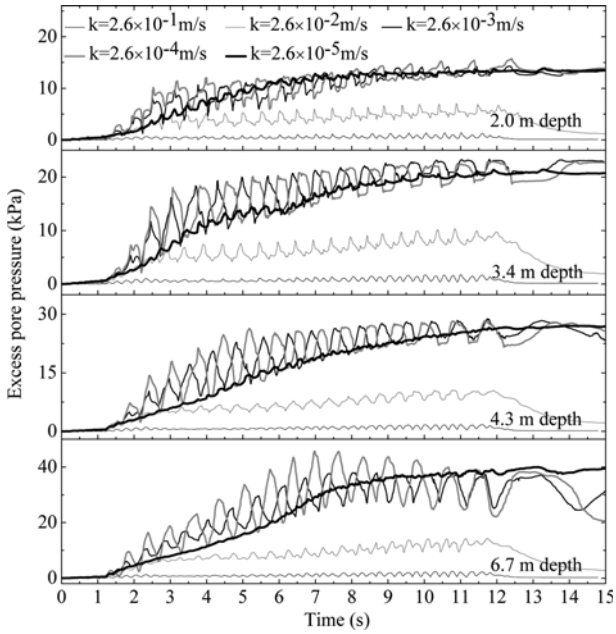

Fig. 11. Influence of the SC Permeability on the Excess Pore Pressures at the Edge

surface acceleration time histories of the silty sand around the SC perimeter for the five cases of different permeability. For the SC with the two highest permeabilities (i.e., 2.6×10^{-1} and 2.6×10^{-2} m/s), the u_e accumulation was low, and the soil did not liquefy. This reduction or lack of u_e accumulation maintained the effective soil confinement and explained why little attenuation behavior was observed at the ground surface as well as the lack of weakening of the soil strength and stiffness during the shaking. These result in a lower u_e because of the good drainage provided by the SCs.

Nevertheless, when the permeability was lower than 2.6×10^{-2} m/s, the influence of the permeability on the u_e in the silty sand was not obvious. The only difference was that the u_e fluctuations and spikes in the cases with permeabilities of 2.6×10^{-3} and 2.6×10^{-4} m/s were more pronounced than in Case SC. In addition, obvious attenuation was observed in the ground surface accelerations for the cases with permeabilities of less than 2.6×10^{-2} m/s.

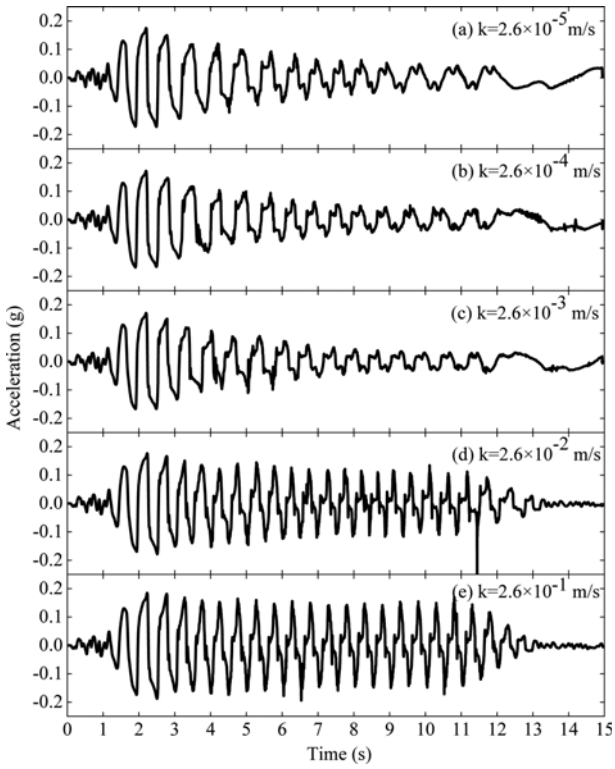

Fig. 12. Influence of the SC Permeability on Surface Accelerations of the Silty Sand at the Edge

Similarly, the reinforcing effects in Case SC effectively reduced the u_e generation in the silty sand below 4.3 m. These effects were similar to those observed in the cases with the permeabilities less than 2.6×10^{-2} m/s, as shown in the u_e response. High permeability could significantly reduce the buildup of u_e in silty sand when the permeability was greater than 2.6×10^{-3} m/s. In addition, liquefaction was completely avoided in the silty sand by the installed SCs with greater permeabilities, which resulted in faster water drainage.

5.4 Influence of Surface Load in the SC Zone

Figures 13 and 14 show the influences of the surface load at the SC zone in the range from 20 kPa to 80 kPa on the excess pore pressures and the ground surface accelerations of the silty sand at the SC edge, respectively.

Overall, slightly stronger surface accelerations were observed in the silt stratum for the cases with relatively larger surface loads (Fig. 14). Likewise, similar behavior of the ground surface accelerations was found under various surface load, which was followed by an attenuation phase due to the u_e accumulation following a few shaking cycles. A larger surface load produced a slight increase in beneficial ground acceleration. Greater surface load slightly enhanced the stiffening effect of the SCs and the transmission (and amplification) of the base accelerations to the surface. Thus, using SC with an increased surface load could enhance the overall foundation stiffness.

Larger loads significantly influenced the u_e at shallower depths

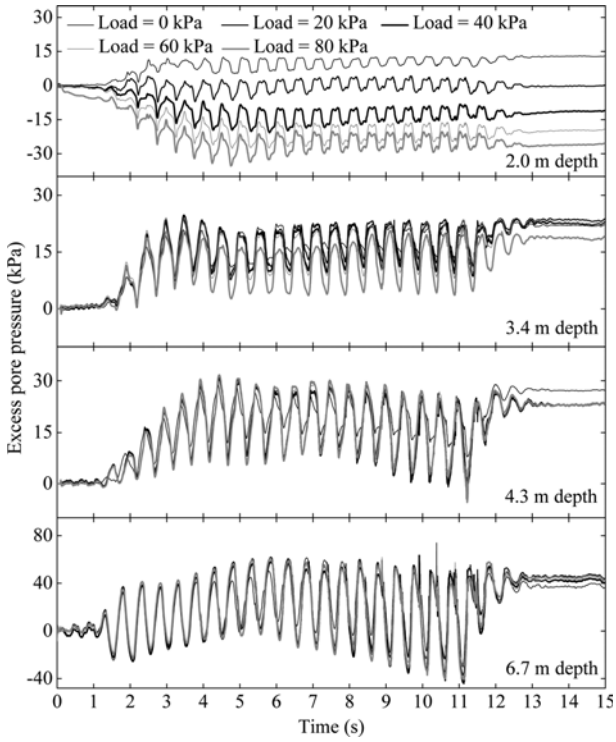

Fig. 13. Influence of the Surface Load on the Excess Pore Pressures of the Silty Sand at the Edge

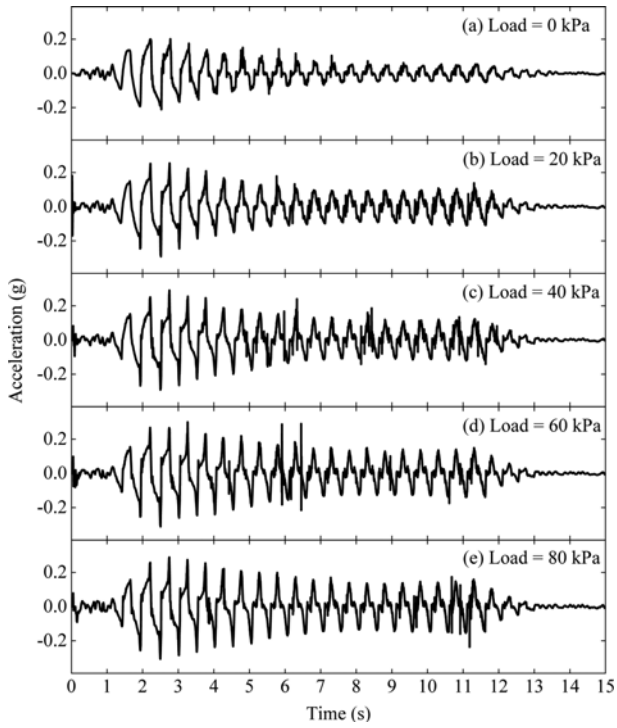

Fig. 14. The Influence of the Surface Load on the Surface Accelerations of the Silty Sand at the Edge

and resulted in a negative u_e trend (Fig. 13). At greater depths, excess pore pressures were insensitive to the surface load. Nevertheless, cyclic mobility was highly enhanced in the silt stratum with increased load, especially at greater depths. An intense negative u_e build-up was observed at the SC perimeter near the ground surface. However, positive u_e spikes were found at greater depths and increased with depth.

6. Conclusions

A 3D FE analysis was conducted to simulate a centrifuge experiment on liquefaction mitigation of silty soils using SCs. The effectiveness of SC mitigation was explored by varying several key parameters. The main findings from this study are summarized below.

1. The FE analysis of the calibrated model produced the dominant liquefaction mechanisms of the SC reinforced silty sand stratum and agreed reasonably with the experimental measurements.
2. The SCs in the silty sand deformed in both flexural and shear modes, in contrast to the current design consideration that assumes pure shear deformation in the SC. In addition, the ratio of the improved to unimproved R_{rd} depended on the vertical and horizontal location.
3. In general, stiffer responses were observed for the SC remediated silty stratum relative to the unimproved stratum. However, full liquefaction in the upper-half silt stratum was not averted.
4. The SCs could substantially retard the build-up of u_e throughout silty stratum and significantly reduced the soil acceleration attenuations when the SC permeability is higher a critical value. Likewise, the SC with low permeability did not effectively inhibit the rise in u_e in the silty sand, especially near the ground surface, thereby not achieving the benefits for mitigating liquefaction hazard.
5. The stiffening benefit due to the larger load applied at the SC zone was slight but produced attenuation-type acceleration once the stratum was fully liquefied. However, the build-up of u_e decreased somewhat with increasing depth.
6. Additional experimental data and parametric studies are needed to explore site-specific liquefaction mitigation strategies with SCs. In addition, a revised design equation should be proposed to estimate the shear stress reduction due to the introduction of the SCs.

Acknowledgements

This research was supported by the National Natural Science Foundation of China (Grant Nos. 51108134 and 51378161), and the Applied Technology Research and Development Plan Program of Heilongjiang Province, China (No. GZ13A009). Prof. Ahmed Elgamal and Dr Jinchi Lu at University of California, San Diego and his team provided the experimental results. These supports are gratefully acknowledged.

Notations

$a_{max,f}$ = The average area-weighted ground surface acceleration

$a_{max,U}$ = The maximum ground surface acceleration
CSR_U = Cyclic shear stress ratio
g = The gravity acceleration
$R_{a,max}$ = The ratio of the maximum ground surface acceleration
R_{CSR} = CSR Reduction Factor
R_{rd} = The ratio of the shear stress reduction coefficient
$r_{d,I}$ = Stress reduction coefficient
$r_{d,U}$ = The shear stress reduction coefficient
$\tau_{s,U}$ = The average cyclic shear stress of the soil
σ'_v = The effective vertical stress of the soil
σ_v = The total vertical stress of the soil
$(\tau_{max})_{d,U}$ = The maximum shear stress
γ' = The total unit weight of the soil
γ_r = Shear strain ratio

References

Adalier, K., Elgamal, A., Meneses, J., and Baez, J. (2003). "Stone columns as liquefaction countermeasure in non-plastic silty soils." *Soil Dynamics and Earthquake Engineering*, Elsevier, Vol. 23, No. 7, pp. 571-584, DOI: 10.1016/S0267-7261(03)00070-8.

Arulmoli, K., Muraleetharan, K. K., Hossain, M. M., and Fruth, L. S. (1992). *VELACS: Verification of liquefaction analysis by centrifuge studies, laboratory testing program, soil data report*, Report, the Earth Technology Corporation, Project No. 90-0562, Irvine, California.

Baez, J. I. (1995). *A design model for the reduction of soil liquefaction by using vibro-stone columns*, PhD Thesis, University of Southern California, Los Angeles.

Baez, J. I. and Martin, G. (1995). "Permeability and shear wave velocity of vibro-replacement stone columns." *Proc. Soil Improvement for Earthquake Hazard Mitigation*, ASCE, San Diego, California, United States, pp. 66-81.

Biot, M. A. (1955). "Theory of elasticity and consolidation for a porous anisotropic solid." *Journal of Applied Physics*, Vol. 26, No. 2, pp. 182-185, DOI: 10.1063/1.1721956.

Elgamal, A., Lu, J., and Forcellini, D. (2009). "Mitigation of liquefaction-induced lateral deformation in a sloping stratum: Three-dimensional numerical simulation." *Journal of Geotechnical and Geoenvironmental Engineering*, ASCE, Vol. 135, No. 11, pp. 1672-1682, DOI: 10.1061/(ASCE)GT.1943-5606.0000137.

Elgamal, A., Yang, Z., Parra, E., and Ragheb, A. (2003)."Modeling of cyclic mobility in saturated cohesionless soils." *International Journal of Plasticity*, Elsevier, Vol. 19, No. 6, pp. 883-905, DOI: 10.1016/S0749-6419(02)00010-4.

Goughnour, R. R. and Pestana, J. M. (1998). "*Mechanical behavior of stone columns under seismic loading*." *Proc. Ground Improvement Techniques*, Singapore, pp. 157-162.

Green, R. A., Olgun, C. G., and Wissmann, K. J. (2008). "Shear stress redistribution as a mechanism to mitigate the risk of liquefaction." *Proc. Geotechnical Earthquake Engineering and Soil Dynamics IV*, ASCE, Sacramento, California, United States, pp. 1-10.

Law, H. K. and Lam, I. P. (2001)."Application of periodic boundary for large pile group." *Journal of Geotechnical and Geoenvironmental Engineering*, ASCE, Vol. 127, No. 10, pp. 889-892, DOI: 10.1061/(ASCE)1090-0241(2001)127:10(889).

Lu, J., Elgamal, A., Yan, L., Law, K. H., and Conte, J. P. (2011)."Large-scale numerical modeling in geotechnical earthquake engineering." *International Journal of Geomechanics*, ASCE, Vol. 11, No. 6, pp. 490-503, DOI: 10.1061/(ASCE)GM.1943-5622.0000042.

Martin II, J. R., Olgun, C. G., Mitchell, J. K., and Durgunoglu, H. T. (2003). "High-modulus columns for liquefaction mitigation." *Journal of Geotechnical and Geoenvironmental Engineering*, ASCE, Vol. 130, No. 6, pp. 561-571, 10.1061/(ASCE)1090-0241(2004)130:6(561).

Mazzoni, S., McKenne, F., Scott, M., and Fenves, G. (2009). *Open System for earthquake engineering simulation user manual Version 2.1.0*., Berkeley, CA, University of California, Pacific Earthquake Engineering Center, USA.

Mitchell, J. K. (2008). "Mitigation of liquefaction potential of silty sands." *Proc. From Research to Practice in Geotechnical Engineering Congress 2008*, Geotechnical Special Publications No. 180, New Orleans, United States, pp. 433-451.

Mitchell, J. K. and Wentz, F. L. (1991). *Performance of improved ground during the loma preita earthquake,* Report No.UCB/EERC-91/12, University of California, Berkeley, California.

Olgun, C. G. and Martin, J. R. (2008). "Numerical modeling of the seismic response of columnar reinforced ground." *Proc. Geotechnical Earthquake Engineering and Soil Dynamics IV*, ASCE, Sacramento, California, United States, pp. 1-11.

Parra, E. (1996). *Numerical modeling of liquefaction and lateral ground deformation including cyclic mobility and dilation response in soil systems*, Ph.D Thesis, Rensselaer Polytechnic Institute, Troy, New York.

Rayamajhi, D., Nguyen, T., Ashford, S., Boulanger, R., Lu, J., Elgamal, A., and Shao, L. (2014). "Numerical study of shear stress distribution for discrete columns in liquefiable soils."*Journal of Geotechnical and Geoenvironmental Engineering,* ASCE, Vol. 140, No. 3, pp. 04013034, DOI: 10.1061/(ASCE)GT.1943-5606.0000970.

Seed, H. B. and Booker, J. (1977). "Stabilization of potentially liquefiable sand deposits using gravel drains." *Geotechnical Engineering Division,* ASCE, Vol. 103, No. 7, pp. 757-768.

Seed, H. B. and Idriss, I. M. (1971). "Simplified procedure for evaluating soil liquefaction potential." *Journal of the Soil Mechanics and Foundations Division,* ASCE, Vol. 97, No. 9, pp. 1249-1273.

Shenthan, T., Nashed, R., Thevanayagam, S., and Martin, G. R. (2004). "Liquefaction mitigation in silty soils using composite stone columns and dynamic compaction."*Earthquake Engineering and Engineering Vibration*, Springer, Vol. 3, No. 1, pp. 39-50, DOI: 10.1007/BF02668849.

Tan, T. S. and Scott, R. F. (1985). "Centrifuge scaling considerations for fluid particle systems." *Geotechnique, ICE Virtual Library*, Vol. 35, No. 4, pp. 461-470, DOI: 10.1680/geot.1985.35.4.461.

Walker, A. J. and Stewart, H. E. (1989). *Cyclic undrained behavior of nonplastic and low plastic silts,* Technical Report, NCEER-89-0035, University at Buffalo, New York.

Yang, Z. (2000). *Numerical modeling of earthquake site response including dilation and liquefaction*, PhD Thesis, Columbia University, New York.

Zienkiewicz, O., Chan, A., Pastor, M., Paul, D., and Shiomi, T. (1990). "Static and dynamic behaviour of soils: A rational approach to quantitative solutions. I. Fully saturated problems." *Proceedings of the Royal Society of London. A. Mathematical and Physical Sciences*, Royal Society Publishing, Vol. 429, No. 1877, pp. 285-309, DOI: 10.1098/rspa.1990.0061.